Critical dynamics at a Hopf bifurcation to oscillatory Rayleigh-Bénard convection

R. E. Ecke, H. Haucke, Y. Maeno,* and J. C. Wheatley
Los Alamos National Laboratory, University of California, Los Alamos, New Mexico 87545
(Received 23 September 1985)

The steady-state and dynamic properties of the transition to oscillatory convection in a low-Prandtl-number fluid, dilute ^{3}He in superfluid ^{4}He, are presented. Critical slowing down is observed and characterized by a phenomenological Landau-Hopf equation in analogy with equilibrium mean-field critical phenomena. In contrast to the onset of classical time-independent Rayleigh-Bénard convection, where appreciable rounding is typically observed, there is no measurable rounding at the oscillatory onset down to a reduced Rayleigh number of 3×10^{-4}. Possible reasons for this are discussed. Different functional singularities are observed for the rms amplitudes of the fundamental and first harmonic spectral components of the oscillation. Finally, the Prandtl-number dependence of the parameters of the dynamics is presented.

I. INTRODUCTION

Instabilities in nonlinear systems far from equilibrium have features in common with equilibrium transitions.[1–3] An example is the onset of classical Rayleigh-Bénard (RB) convection which has been successfully described using a phenomenological Landau-Hopf equation with the magnitude of the convective velocity acting as an effective order parameter. Both the square-root behavior of the velocity amplitude and the inverse dependence of the characteristic time for relaxation of transients on reduced stress parameter are clearly observed in many different fluid systems.[4–7] Sneddon[8] further strengthened the connection between the RB instability and an equilibrium phase transition. He pointed out that contrary to previous descriptions[9] the broken symmetry at the onset of stationary convection is discrete velocity-reversal symmetry rather than continuous spatial-translation symmetry. He also noted the symmetry-breaking properties of lateral side-wall heating and its effect on the transition.

Another instability common in low-Prandtl-number convection is a continuous transition from a time-independent state to an oscillatory state. The steady-state and transient behavior in the vicinity of this bifurcation has been studied qualitatively by Libchaber and Maurer[10] and in more detail by Ecke *et al.*[11] An analogous transition to wavy Taylor-Couette flow was studied by Pfister and Gerdts.[12] Here we present a description of the transition to oscillatory convection in a dilute solution of ^{3}He in superfluid ^{4}He. We also apply a phenomenological equation which describes the transition very well. The equation is related to similar amplitude equations derived from a mode truncation of the Boussinesq equations for low-Prandtl-number oscillatory convection.[13] The resulting picture is a classic example of a mean-field nonequilibrium phase transition. One can also consider this transition as a forward Hopf bifurcation since a new time-dependent periodic mode grows continuously from zero amplitude.

The fluid with which we study oscillatory RB convection is a dilute solution of 1.46% ^{3}He in superfluid ^{4}He. These solutions have been shown experimentally to undergo effectively single-component convection.[14,15] A theoretical description[16,17] predicts negligibly small two-fluid corrections. The Prandtl number σ is both low and variable ($0.04\rightarrow0.15$). No other fluid's Prandtl number falls in the same regime. The variability of almost a factor of 4 in σ allows for the determination of how the instabilities in the system depend on Prandtl number. The low-σ characteristic leads to primarily time-dependent instabilities as opposed to stationary spatial pattern transitions seen in higher-σ fluids.[18] We emphasize high-precision measurements of these temporal instabilities since our cryogenic environment allows for excellent stability and low intrinsic noise. The disadvantage is a lack of flow visualization.

In this system the first instability, a transition from diffusive thermal conduction to stationary (time-independent) RB convection, occurs at a critical Rayleigh number R_c. At higher Rayleigh number a bifurcation to a limit cycle (single-frequency oscillatory state) is observed. While the first instability point depends only slightly (if at all) on Prandtl number, the onset of oscillations is strongly Prandtl-number dependent.[14,15] Figure 1 shows the Rayleigh-Prandtl number parameter space for these instabilities. Instabilities at higher Rayleigh number are described elsewhere.[19,20]

The two dimensionless parameters mentioned above which characterize the convective state are the Rayleigh number R and the Prandtl number σ. They are defined as

$$R=\frac{g\beta\Delta T d^3}{\nu\kappa} \text{ and } \sigma=\nu/\kappa\ , \tag{1}$$

where g is the acceleration of gravity, β is the thermal expansion coefficient, ΔT is the top-bottom temperature difference, d is the cell height, ν is the kinematic viscosity, and κ is the thermal diffusivity. The precise definition of these fluid parameters for ^{3}He-^{4}He solutions is described elsewhere.[15]

An additional factor which determines the types of convective motion is the aspect ratio. We employ a small-

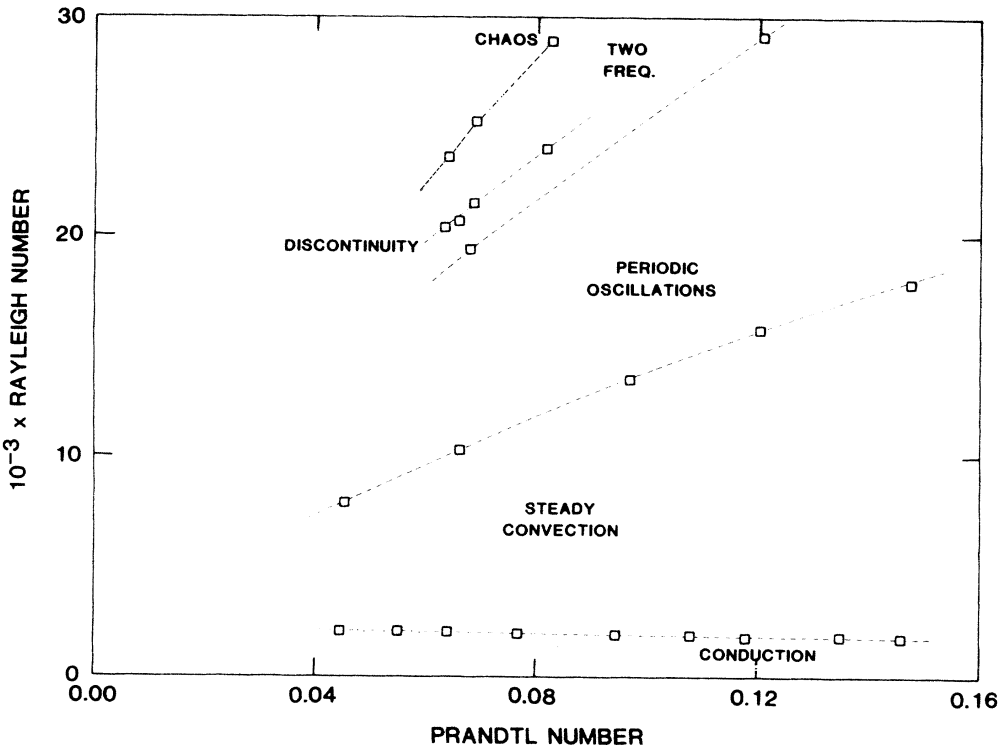

FIG. 1. Rayleigh-Prandtl number parameter space.

aspect-ratio rectangular geometry with aspect ratios $\Gamma \equiv L/2d = 1.0$ and $\Gamma' \equiv W/2d = 0.70$ where $d = 0.80$ cm is the cell height and $L = 1.60$ cm and $W = 1.12$ cm are the longer and shorter lateral sides, respectively. In contrast to large aspect ratio convection where unstable roll structures are typical,[21] the lateral side walls in small-aspect-ratio cells serve to limit the possible roll wavelengths. The roll patterns are usually two-dimensional with the number of rolls dependent on the precise geometry.

In our cell there are several quite distinct stationary convective states which probably correspond to different spatial roll structures.[15,22] Here we study the state with the highest effective heat-transport efficiency. Although we have no direct observations of the spatial patterns, we have some evidence that this state corresponds to two parallel rolls oriented perpendicular to the longer of the side boundaries with fluid rising in the center.

II. EXPERIMENT

Although an extensive description of the experimental apparatus and techniques has been presented elsewhere,[15] a brief version is given here. The RB cell in Fig. 2 consists of copper top and bottom plates, a cylindrical stainless-steel can which confines the fluid and a Vespel[23] graphite polymide-resin insert of low thermal conductance which defines the cell geometry. The geometry is rectangular with dimensions 0.80 cm in height and 1.60 cm and 1.12 cm for the longer and shorter sides, respectively.

There is a small ($\sim 4\%$ of cell top-plate area) thermally insulated copper probe located at the center of the cell top plate which allows for local thermal measurements via a Au-Fe thermocouple[15,24] which is sensed by a superconducting quantum interference device ammeter. As fluid motion occurs in the cell, heat fluxes will be different for the probe and top plate thereby inducing temperature differences measured by the probe thermocouple.

There are germanium resistance thermometers (GRT's) on the top and bottom plates which measure absolute temperature. The bottom plate is temperature controlled, and a constant heat flow is applied to the top plate (due to the negative thermal expansion coefficient of the solutions[15]). The top GRT is used to determine the top-bottom temperature difference ΔT. For time-dependent convective states ΔT fluctuates so that both ΔT and R are defined as time averages.

The cell was attached to a continuously operating ^{3}He evaporation refrigerator whose dynamic operating range was 0.4 to 1.5 K. In practice the cell temperature was set between 0.7 and 1.1 K to obtain the desired fluid Prandtl number between 0.04 and 0.15. The majority of the work presented here is for a bottom-plate temperature of 0.850 K, a mean cell temperature of 0.876 K, a corresponding σ of 0.066, and a critical Rayleigh number R_c for the onset of stationary convection of 2017 ± 140.

III. DATA

In our previous work[11] on the dynamics near the oscillatory onset we measured the output of the probe thermocouple after a sudden change in top-plate heat flow. The rms steady-state oscillatory amplitude was observed to increase linearly with R above R_0 (Refs. 11 and 14) where

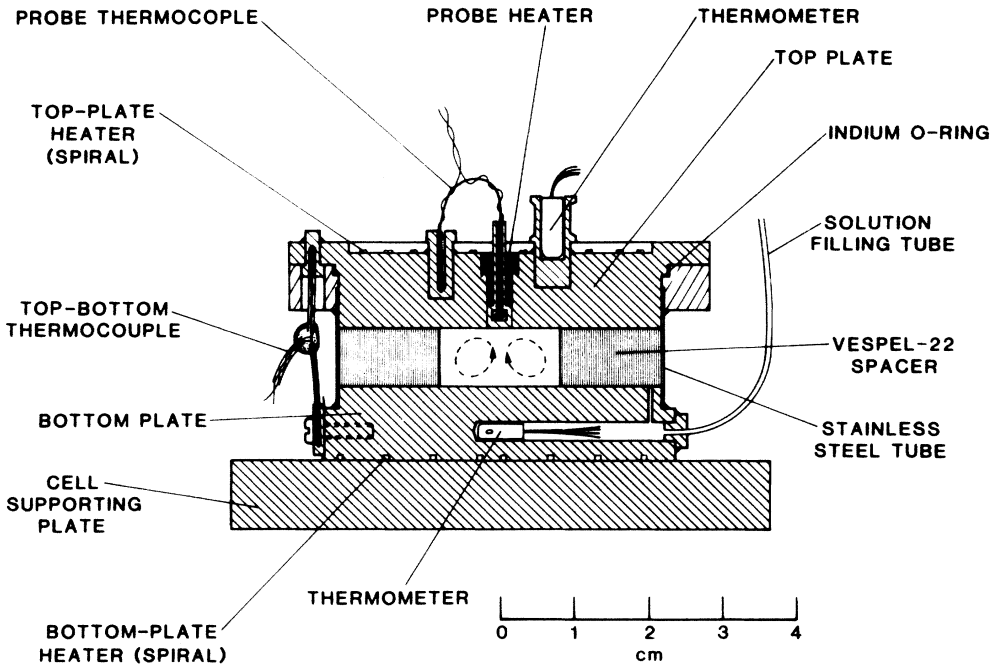

FIG. 2. Rayleigh-Benard convection cell.

R_0 is the onset Rayleigh number. The oscillation frequency increases as $(R-R_c)^{1/2}$ and is 0.45 Hz at onset for $\sigma=0.066$. The rms amplitude of the oscillation decays to a new steady-state value with a characteristic relaxation time which diverges as R_0 is approached from either above or below. To measure quantitatively the relaxation time we digitally recorded the probe-temperature oscillations using a 12-bit analog-to-digital converter. The oscillation envelope was then numerically fit by a nonlinear equation which described the linear increase of the steady-state amplitude with R (as discussed below). We obtained good agreement between the phenomenological equation and the static and dynamic data. However the scatter in the oscillation envelope was too large for good stability in the curve fitting. In fact, below onset we had to use an asymptotic exponential equation rather than the full nonlinear equation. Here we describe an improved method for measuring the relaxation which dramatically increases the signal-to-noise ratio. The lower noise combined with higher system stability allows for measurements almost a factor of 100 closer to onset.

The method we employ here to measure the relaxation of the oscillations is as follows: First the oscillatory state is allowed to relax to a steady state above onset, at $R/R_c=5.35$. Next, the top-plate heat flow is suddenly decreased so that the resultant R is decreased to a value either above or below onset. Immediately following the sudden decrease in heat flow, there is a rapid change in the measured top-bottom temperature difference which has a characteristic time τ_c. This characteristic time, probably due to thermally diffusive relaxation and to relaxation of the stationary convective velocity, is independent of R to experimental accuracy over the transition region. For the 0.85 K ($\sigma=0.066$) data $\tau_c=2.3\pm0.2$ sec. This is to be compared to the vertical thermal diffusion time $\tau_\kappa\equiv d^2/\pi^2\kappa=3.8$ sec at 0.85 K. After a time greater than $4\tau_c$, we record the transient response, amplified and filtered by a Princeton Applied Research 113 preamp with a low pass of 3 Hz and a high pass of 1 Hz. The high-pass filter was used to avoid saturation of the preamp due to the large nonoscillatory change of the probe output associated with the rapid relaxation described above. The frequency response of the preamp was measured and all rms amplitudes reported in this paper are correctly compensated. Two time series of the measured probe output which illustrate the transient response are shown in Figs. 3(a), $R/R_c=5.138$, above onset and 3(c), $R/R_c=5.082$, below onset. To obtain a better signal-to-noise ratio we divide the time series into segments and obtain via a fast Fourier transform the power spectral density for each segment. From the power under one of the spectral peaks in a frequency interval of about 0.5 mHz we obtain a narrow-banded rms amplitude for that frequency component. Since the change in the frequency over each segment is small and the period of the oscillations is short compared to the relaxation time, the measured rms amplitude is a good representation of the relaxation of the oscillations. In Fig. 4, two power spectra, uncorrected for the frequency response of the preamp, are shown. The upper figure is for $R/R_c=5.250$ which represents the largest value of R/R_c studied. The bottom power spectrum is for an $R/R_c=5.150$, much closer to onset. Close to onset only the f and $2f$ components are visible while further away higher harmonics appear. Both spectra have less background noise at $2f$ than at f. By considering just the $2f$ harmonic and dividing the transient time series into segments as discussed above, we obtain the rms amplitudes in Figs. 3(b) and 3(d) for the corresponding time

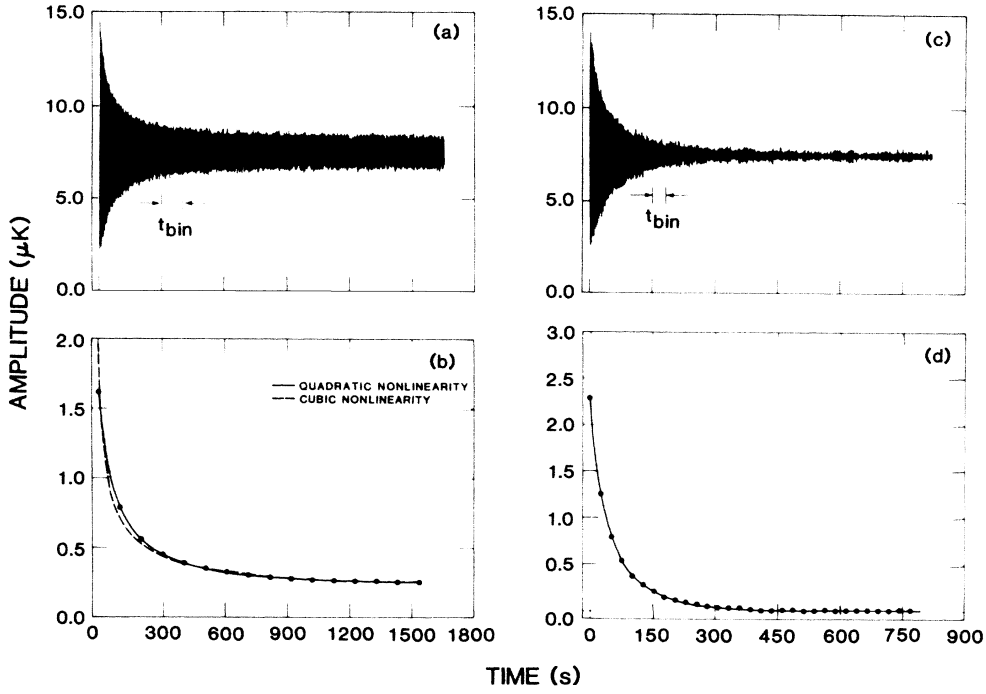

FIG. 3. Transient time series for (a) $R/R_c = 5.14$ and (c) $R/R_c = 5.08$. The binning times are about 100 sec for (a) and 30 sec for (c). Spectrally binned data (b) and (d) for time series (a) and (c), respectively, with quadratic nonlinear fits as solid lines and the cubic nonlinearity as a dashed line in (b).

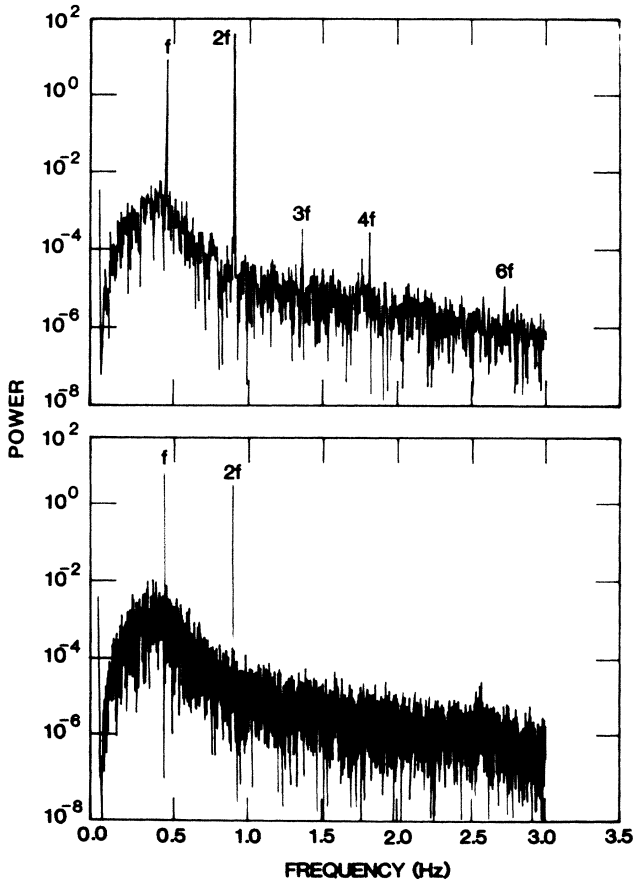

FIG. 4. Power spectral density of oscillations at $R/R_c = 5.25$ and 5.15 for upper and lower figures, respectively.

series. The solid and dashed lines in Fig. 3 are fits to the data as discussed below.

IV. ANALYSIS

The quantity measured in our experiment, the probe top-plate temperature difference $\delta T(t)$, is not necessarily simply related to more fundamental measures of the oscillatory convective state such as the oscillatory component of the convective velocity. McLaughlin and Martin[13] studied low-Prandtl-number convection and calculated various convective modes which vary as different powers of the oscillatory velocity. Our measurement probably couples to different modes and therefore might be expressible in terms of a power-series expansion of $\delta T(t)$,

$$\delta T(t) = C_1 v(t) + C_2 v^2(t) + \cdots , \tag{2}$$

where $v(t)$ is the oscillatory convective velocity and C_1 and C_2 are constants which may depend on σ. Suppose that the oscillatory velocity is composed only of the fundamental f and furthermore has a cubic nonlinearity as for a typical Landau-Hopf singularity. If the amplitude relaxes slowly with respect to the oscillation frequency then we can write

$$v(t) = v_0(t)\cos(\omega t) , \tag{3}$$

where $v_0(t)$ is the rms oscillatory velocity amplitude and satisfies

$$\frac{dv_0}{dt} = r(R - R_0)v_0 - s v_0^3 . \tag{4}$$

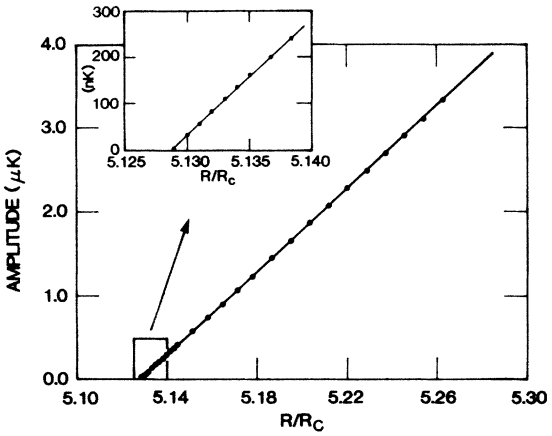

FIG. 5. The rms amplitude of the $2f$ harmonic plotted in units of 10^{-6} K vs R/R_c where $R_c=2017$. Inset is in units of 10^{-9} K.

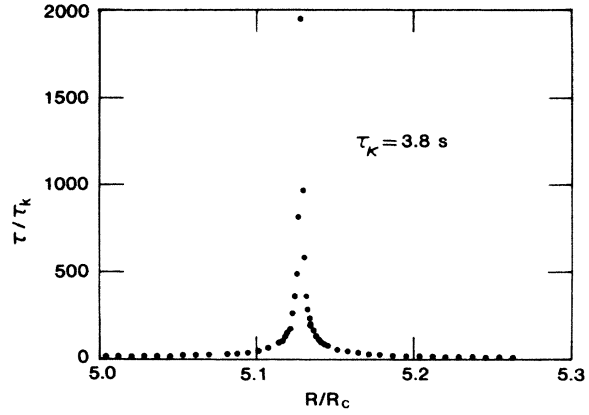

FIG. 6. Relaxation time for the transient relaxation of the $2f$ harmonic of the rms oscillatory amplitude. Here $\tau_\kappa=3.8$ sec and $R_c=2017$.

The constants r and s are taken to be positive. Combining the leading terms in Eq. (2) with Eq. (3) and using $\cos^2(\omega t)=[1+\cos(2\omega t)]/2$, we obtain

$$\delta T(t)=\frac{C_2}{2}v_0^2(t)+C_1 v_0(t)\cos(\omega t)+\frac{C_2}{2}v_0^2(t)\cos(2\omega t)\ . \tag{5}$$

Let $A(t)$ and $B(t)$ be the rms amplitudes of the f and $2f$ components of $\delta T(t)$. From Eq. (5) we get $A(t)=C_1 v_0(t)$ and $B(t)=C_2 v_0^2(t)/2$ where $A(t)$ and $B(t)$ satisfy the dynamic equations

$$\frac{dA(t)}{dt}=r(R-R_0)A-(s/C_1^2)A^3 \tag{6}$$

and

$$\frac{dB(t)}{dt}=2r(R-R_0)B-(4s/C_2)B^2\ . \tag{7}$$

These equations can be explicitly integrated to get

$$A(t)=\left[\gamma_1^2+\left[\frac{1}{A^2(0)}-\gamma_1^2\right]e^{\mp 2t/\tau_1}\right]^{-1/2} \tag{8}$$

and

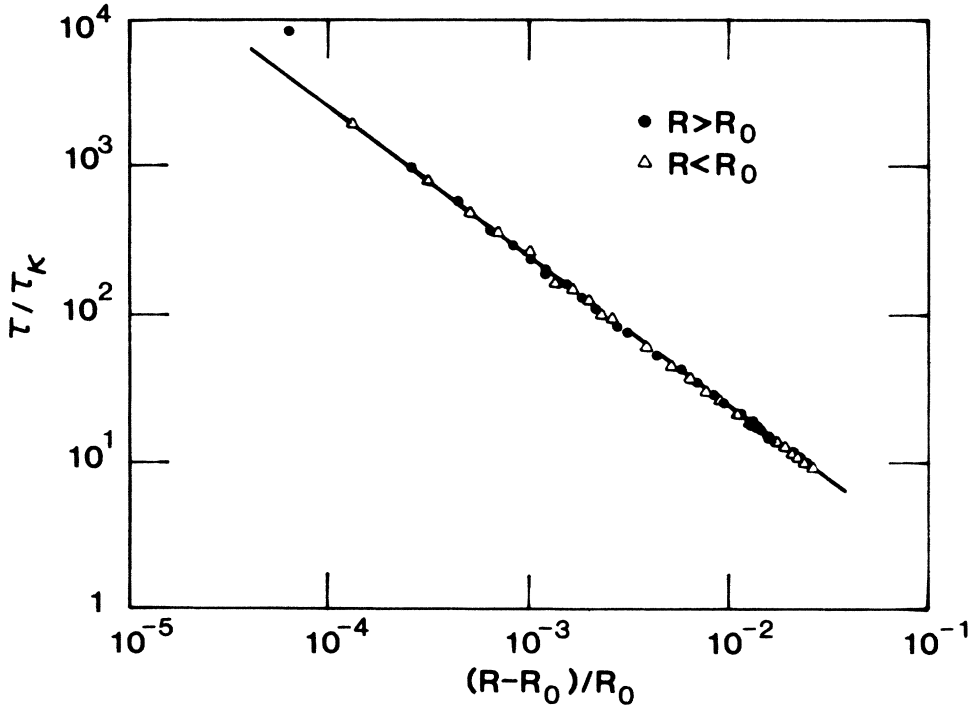

FIG. 7. τ/τ_κ plotted versus reduced Rayleigh number, $(R-R_0)/R_0$ where $R_0=10\,344.3$ and $\tau_\kappa=3.8$ sec. Data points, ●, correspond to $R>R_0$ and △ to $R<R_0$.

$$B(t)=\left[\gamma_2+\left[\frac{1}{B(0)}-\gamma_2\right]e^{\mp t/\tau_2}\right]^{-1}, \quad (9)$$

where $\tau_1 \equiv 1/r\,|R-R_0|$, $\tau_2 \equiv 1/2r\,|R-R_0|$, $\gamma_1 \equiv s/rC_1(R-R_0)$, and $\gamma_2 \equiv s/rC_2(R-R_0)$. For later convenience we define $\tau \equiv \tau_2 = \tau_1/2$. The $-$ and $+$ in the exponential factor correspond to above and below onset respectively. Above onset, $\gamma_1 = 1/A^2(\infty)$ and $\gamma_2 = 1/B(\infty)$ which gives a square-root dependence of the rms amplitude of the f component on R and a linear dependence of the $2f$ rms amplitude on R. Also, there is a divergence in the relaxation time of the form $(R-R_0)^{-1}$. In a stationary Taylor-Couette flow experiment Gollub and Freilich[7] studied the different singular dependences of spatial Fourier modes of the velocity field. They observed some agreement with the prediction[25] that the asymptotic (close to onset) limit of the expansion coefficients should scale as $p/2$ where p labels the pth Fourier coefficient. For $p=1$ they obtain 0.5 but the second mode gives 0.76 rather than one. Here we have performed a similar time Fourier expansion of an oscillatory convective temperature mode. The first and second Fourier coefficients of the oscillatory temperature amplitude should have square-root and linear dependences, respectively, as described above.

We consider the behavior of the $2f$ rms amplitude data first because of the lower system noise at that frequency. The transient time series, recorded as described above, is numerically fit to an equation of the form of Eq. (9) with an additional term which represents the system noise. We suppose that the noise is uncorrelated with the oscillation amplitude. Therefore we use a fitting equation of the form

$$E(t)=[B^2(t)+N^2]^{1/2}, \quad (10)$$

where $E(t)$ is the experimentally measured probe output and N is an rms-averaged noise constant. The additional noise term is essential for obtaining a good fit below onset since the experimental time series has a finite rms amplitude even at large times due to the noise.

The transient time series for the $2f$ component are fit very well by Eq. (10) as seen in Figs. 3(b) and 3(d), where the solid lines are the numerical fits. For comparison a fit

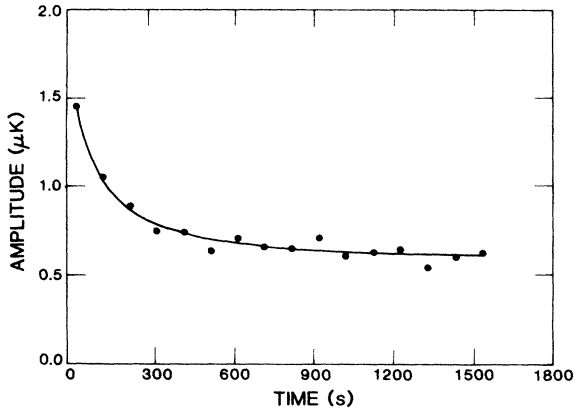

FIG. 8. Spectrally binned transient time series for rms amplitude of the f spectral component and the fit (solid line) to an equation with cubic nonlinearity.

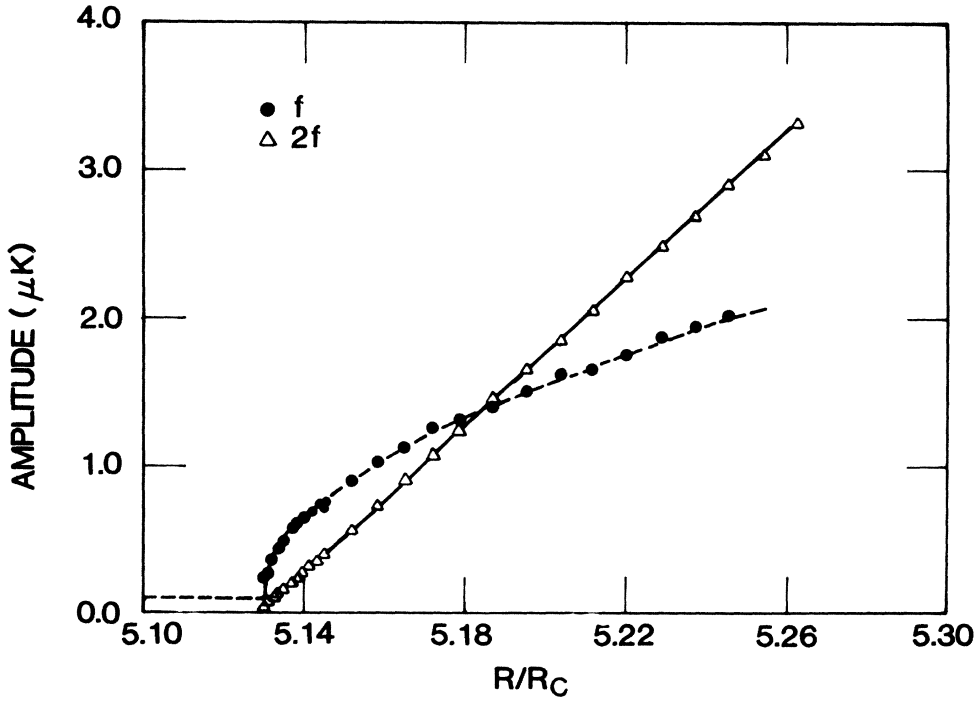

FIG. 9. The rms amplitudes for the f (●) and $2f$ (△) components of the oscillation. Here $R_c = 2017$. The dashed line below onset is the average rms noise at the frequency f. Above onset, the dashed line is a guide to the eye and the solid line is the least-squares fit described in the text.

to an equation of the form of Eq. (8) which has a cubic nonlinearity with an added noise as in Eq. (10) is perceptibly inferior, dashed line in Fig. 3(b); an exponential is far worse. From the fits to an equation with quadratic nonlinearity plus noise, Eq. (10), we obtain the steady-state amplitude above onset and the characteristic time both above and below onset. The steady-state amplitude is very stable with respect to the fitting procedure since in most cases the last part of the time series has reached a steady state. The error in the amplitude is estimated at 1%. Figure 5 shows the rms amplitude of the $2f$ component as a function of R/R_c where $R_c=2017$. The rms noise amplitude N was determined to be $(6\pm3)\times10^{-9}$ K. The linear dependence of the amplitude on R is in agreement with the fitting equation; a power law fit yields 0.996 ± 0.005. Also, there is no perceptible rounding, inset of Fig. 5, in the vicinity of onset down to within $(R-R_0)/R_0\sim3\times10^{-4}$, where the Rayleigh number at onset, R_0, is determined to be 10 344.3 from a linear least-squares fit to the steady-state amplitude data. In our system the onset of stationary convection is rounded at $(R-R_c)/R_c\simeq10^{-2}$. This rounding may be attributable to imperfections in the cell boundary conditions such as variations in cell height. Such imperfections would also seem likely to round the oscillatory onset. The fact that we observe much less rounding at the oscillatory onset suggests that either the region driving the oscillations is spatially localized or that some boundary condition couples differently to the different transitions. There is evidence that the oscillation does have some localized properties.[22] From another perspective, side-wall heating can act as a symmetry-breaking field for stationary convection and cause an imperfect, rounded bifurcation. However,

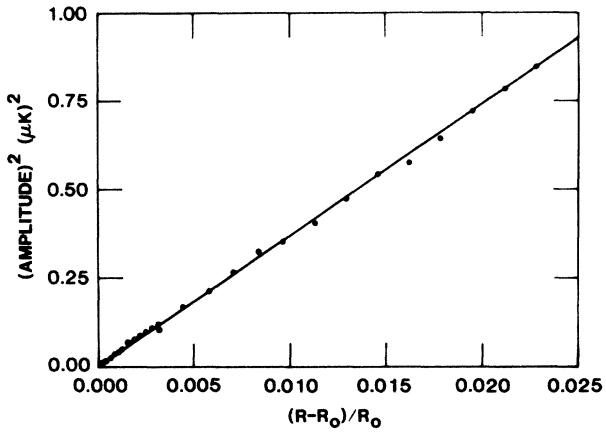

FIG. 10. The rms amplitude squared of the f component of the oscillation vs $(R-R_0)/R_0$ where $R_0=10\,344.3$.

for the oscillatory onset the analogous symmetry-breaking field would be periodic side-wall heating; the phase of the periodic field would break the continuous phase symmetry of the oscillatory state. In other words, the constant side-wall heating breaks the velocity-reversal symmetry for the stationary state but does not affect the oscillatory state. One could in principle test this hypothesis as suggested by Sneddon.[8] We plan to investigate the effects of periodically forced side-wall heating as a symmetry-breaking field for the oscillatory onset. Until such time we have no way to distinguish whether localized driving or side-wall heating is responsible for the differences in rounding between the stationary and oscillatory instabilities.

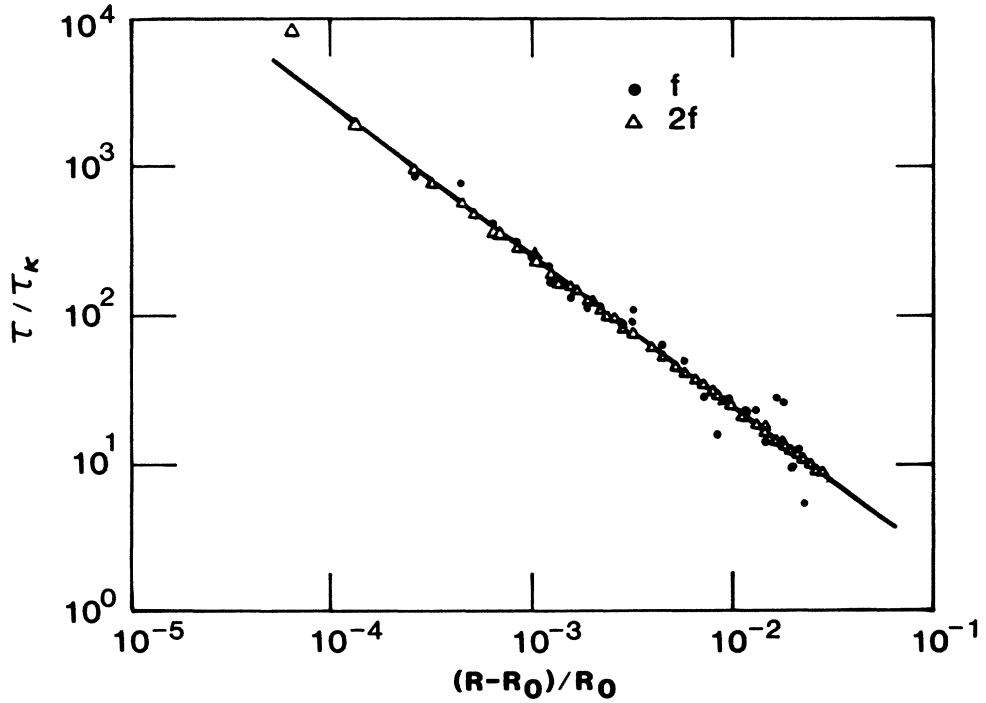

FIG. 11. τ/τ_κ plotted vs $(R-R_0)/R_0$ were $\tau_\kappa=3.8$ sec and $R_0=10\,344.3$ for the fundamental, f (●) and the first harmonic, $2f$ (△).

TABLE I. Prandtl-number dependence of dynamical parameters.

σ	R_0	τ_κ (sec)	f_0 (Hz)	z	τ_0/τ_κ
0.0454	7898.0	2.09	0.617	1.01±0.01	0.315±0.005
0.0661	10344.3	3.80	0.448	1.003±0.004	0.247±0.002
0.0979	13511.0	6.50	0.316	1.01±0.01	0.199±0.005
0.1203	15694.3	9.27	0.266	1.01±0.01	0.181±0.004
0.1476	17911.6	13.27	0.215	1.01±0.01	0.142±0.005

The characteristic time, as measured from analysis of the transient time series of the $2f$ spectral component, diverges at the onset, see Fig. 6. A divergence of the form $\tau=\tau_0[(R-R_0)/R_0]^{-z}$ is expected from Eq. (9) with $z=1$. To determine z and τ_0 from the data we plot, Fig. 7, $\log_{10}$ of τ/τ_κ, where τ_κ is the vertical thermal diffusion time, vs $\log_{10}$ of $(R-R_0)/R_0$. The data above and below onset fall on a single curve with $z=1.003\pm0.004$ and $\tau_0/\tau_\kappa=0.247\pm0.003$. The point closest to R_0 was not used due to its 50% uncertainty compared to 10% for other values of τ. The value of R_0 which was used corresponds to the one obtained from a least-squares fit to the steady-state amplitude data, $R_0=10344.3\pm5$. R_0 was varied within these error bars to obtain the best agreement in terms of the time constant data above and below onset falling on one curve. Actually, the final value used was the steady-state value given above but that is probably fortuitous considering the error bars. The data very close to R_0 make the $\log_{10}$ plot very sensitive to the value of R_0 so that variations of as little as $\Delta R_0\sim0.5$ affected the fit. Fitting each region separately yielded values of $z^+=1.000\pm0.004$, $z^-=1.008\pm0.006$, $\tau_0^+/\tau_\kappa=0.250\pm0.003$, and $\tau_0^-/\tau_\kappa=0.242\pm0.005$ where $+$ and $-$ refer to above and below onset, respectively. The value of z very close to one is further confirmation of the validity of the nonlinear equation used in the fits.

There are two points which need to be mentioned regarding the use of the Rayleigh number as the independent variable in our analysis. First, one must be sure that the state of the oscillations is determined only by its final state value of R. This will be true provided the gross convective and thermal flows relax quickly on a time scale set by the relaxation time of the oscillatory amplitude. The oscillatory frequency should act as a measure of the relaxation of the major flows. We observe that the oscillatory frequency relaxes quickly to a value close to its steady-state value but does change further by a small amount as the amplitude relaxes. This is a small second-order effect which brings us to the second point regarding R. As mentioned earlier, R is a time-averaged quantity whose rms-averaged value is a function of the oscillatory amplitude. Actually the voltage applied to the top-plate heater is a better measure of the boundary conditions but not necessarily a better measure of the state of the fluid flows which depends on R; besides R is a more intuitive parameter for describing the state of the system. Therefore, we fit R as a function of heater voltage over the region of interest and use the interpolated values of R in the analysis. Only close to onset where the oscillatory amplitude decays slowly is there substantial deviation from a smooth fit; the fractional deviation is only about 1% to 2%.

According to the phenomenological description above, Eqs. (2)–(9), the rms amplitude of the f component of the oscillation should have a square-root dependence on $R-R_0$. The increased scatter in the f rms amplitude, Fig. 8, makes fitting less reliable; fits to either quadratic or cubic nonlinearities give similar results. However, fits to Eq. (8), which corresponds to the cubic nonlinearity, yield the square-root amplitude dependence, Figs. 9 and 10, and the same characteristic dependence of response time on $R-R_0$, Fig. 11, as the $2f$ component. The values of τ plotted in Fig. 11 are $\tau=\tau_2=\tau_1/2$ from Eqs. (8) and (9). A power law fit to the steady-state rms amplitude of the f component vs $R-R_0$ yields an exponent 0.48 ± 0.05. Fitting to Eq. (9), corresponding to a quadratic nonlinearity, also yields the square-root dependence of the rms amplitude in contrast to the linear dependence predicted by the fitting equation and yields values of the characteristic time which show no relation to the values obtained for the $2f$ component. The dashed line below the onset in Fig. 9 represents the fitted value of N which is about 6×10^{-8} K, an order of magnitude larger than for the $2f$ component.

From the analysis, Eqs. (2)–(9), which leads to the correct description of both the f and $2f$ components, we should also expect a nonoscillatory component which decays with the same time constant. Although we qualitatively observed this phenomenon, no quantitative analysis was attempted since for the data presented here the preamp high-pass filter at 1 Hz effectively kills the nonoscillatory component. Another point related to the analysis is that it was observed experimentally that as the higher harmonics start to become visible, as in Fig. 4, the dependence of the rms amplitude of the $2f$ component on

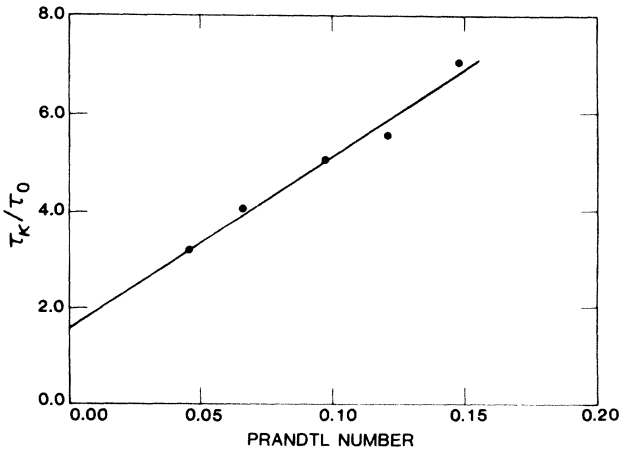

FIG. 12. τ_κ/τ_0 plotted versus Prandtl number.

$R-R_0$ departs from linearity. This observation is consistent with the picture described above since the next higher term in the expansion, Eq. (2), is $\cos^3(\omega t)$ which contributes a different nonlinear part to both the f and $2f$ components.

Finally, we consider the Prandtl-number dependence of the parameters which describe the dynamics. We restrict ourselves to the $2f$ components for simplicity. The Prandtl-number dependence of R_0 was previously studied[14] and can be seen in Fig. 1 for the new data reported here. Table I shows values of σ, R_0, τ_κ, f_0 (the oscillation frequency at onset), z, and τ_0/τ_κ (z and τ_0/τ_κ are the average for both $R<R_0$ and $R>R_0$) for five different data sets. The larger errors in z and τ_0/τ_κ, for the data at temperatures other than at 0.85 K stem from the coarser detail used to study the transients at those temperatures. Also in several cases the range of reduced R contains substantial higher harmonic content indicating a breakdown of the simple decomposition of Eq. (5). The variation of τ_κ/τ_0 vs σ is plotted in Fig. 12 and indicates that τ_0 is varying roughly as $1/\sigma$. A linear least-squares fit to an equation of the form $\tau_\kappa/\tau_0=m\sigma+l$ yields $m=36\pm3$ and $l=1.6\pm0.2$. A theoretical description of low-Prandtl-number oscillatory convection due to McLaughlin and Martin[13] predicts a linear dependence of τ_0 on σ in contradiction to the $1/\sigma$ dependence we observe.

V. CONCLUSIONS

We have drawn a detailed and precise picture of the static and dynamic response of an oscillatory convective state near a forward Hopf bifurcation. The different singularities of the rms amplitudes of the fundamental and first harmonic are probably a consequence of the particular way in which we obtain the oscillatory probe temperature signal. The exponent of the characteristic relaxation time is $z=1.003\pm0.004$ for the extensively studied data set corresponding to $\sigma=0.066$ and $z=1.01\pm0.01$ for the other mean cell temperatures studied. This dynamic exponent is reminiscent of classic dynamic relaxation in equilibrium critical phenomena for mean-field phase transitions. Since critical fluctuations are small near hydrodynamic bifurcations[26] one expects the mean-field behavior which is observed.

Direct observations of intrinsic noise amplification near the bifurcation point are beyond the range of this experiment, primarily due to the critical slowing down which makes observations at small $(R-R_0)/R_0$ untenable in practice. However, the growth rate of the oscillations when the system is changed from a state below onset to one above onset may given an indication of the intrinsic noise of the initial state. Preliminary measurements indicate a much lower intrinsic noise than the measured experimental noise background.

Finally, the Prandtl-number dependences of the dynamic parameters, i.e., τ_0 and z, are obtained. No theoretical framework exists to explain the inverse dependence of τ_0/τ_κ on σ.

Note added in proof. It has been pointed out to us by Busse that since the toroidal velocity field is the main component of the oscillatory motion,[27] the dynamics should be governed by the characteristic relaxation time for vorticity, τ_ν. Since $\tau_\nu\equiv d^2/\nu$ we get $\tau_\nu=\tau_\kappa/\sigma$ with ν, d, σ, τ_0, and τ_κ defined in the text.

ACKNOWLEDGMENTS

We acknowledge much helpful assistance from G. Swift, S. Buchanan, and A. Migliori. We also benefited from discussions with L. Sneddon and are grateful to G. Ahlers for bringing some relevant work to our attention. Work at Los Alamos was performed under the auspices of the U. S. Department of Energy.

*Present address: Department of Physics, Faculty of Science, Hiroshima University, Hiroshima 730, Japan.

[1]C. Normand, Y. Pomeau, and N. Velarde, Rev. Mod. Phys. **49**, 581 (1977).
[2]P. W. Anderson, *Basic Notions of Condensed Matter Physics* (Benjamin/Cummings, California, 1984).
[3]R. Graham, in *Fluctuations, Instabilities, and Phase Transitions,* edited by T. Riste (Plenum, New York, 1975), p. 215.
[4]R. Behringer and G. Ahlers, Phys. Lett. **62A**, 329 (1977).
[5]J. Weisfreid, Y. Pomeau, M. Dubois, C. Normand, and P. Berge, J. Phys. Lett. (Paris) **39**, L725 (1978).
[6]Y. Sawada, Phys. Lett. **65A**, 5 (1978).
[7]J. P. Gollub and M. H. Freilich, Phys. Fluids **19**, 619 (1976).
[8]L. Sneddon, Phys. Rev. A **24**, 1629 (1981).
[9]H. Haken, *Synergetics, An Introduction* (Springer, Berlin, 1977).
[10]A. Libchaber and J. Maurer, in *Proceedings of the NATO Advanced Study Institute on Nonlinear Phenomena at Transitions and Instabilities,* edited by T. Riste (Plenum, New York, 1981).
[11]R. E. Ecke, Y. Maeno, H. Haucke, and J. Wheatley, Phys. Rev. Lett. **53**, 1567 (1984).
[12]G. Pfister and U. Gerdts, Phys. Lett. **83A**, 23 (1981).
[13]J. McLaughlin and P. Martin, Phys. Rev. A **12**, 186 (1975).
[14]Y. Maeno, H. Haucke, and J. Wheatley, Phys. Rev. Lett. **54**, 340 (1985).
[15]Y. Maeno, H. Haucke, R. E. Ecke, and J. Wheatley, J. Low Temp. Phys. **59**, 305 (1985).
[16]A. Fetter, Phys. Rev. B **26**, 1164 (1982); **26**, 1174 (1982).
[17]V. Steinberg, Phys. Rev. A **24**, 975 (1981).
[18]F. H. Busse, Rep. Prog. Phys. **41**, 1929 (1978).
[19]H. Haucke, R. E. Ecke, Y. Maeno, and J. Wheatley, Phys. Rev. Lett. **53**, 2090 (1984).
[20]H. Haucke and R. E. Ecke (unpublished).
[21]M. S. Heutmaker, P. N. Fraenkel, and J. P. Gollub, Phys. Rev. Lett. **54**, 1369 (1985); G. Ahlers, D. S. Cannell, and V. Steinberg, *ibid.* **54**, 1373 (1985); M. C. Cross, Phys. Rev. A **25**, 1065 (1982).
[22]Y. Maeno, H. Haucke, R. E. Ecke, and J. Wheatley, in *Proceedings of the 17th International Conference on Low Temperature Physics,* edited by U. Eckern, A. Schmid, W. Weber, and H. Wühls (Elsevier, Amsterdam, 1984), p. 1123.
[23]Dupont, Wilmington, Delaware.
[24]Y. Maeno, H. Haucke, and J. Wheatley, Rev. Sci. Instrum. **54**, 946 (1983).
[25]A. Davey, J. Fluid Mech. **14**, 336 (1962).
[26]R. Graham, Phys. Rev. A **10**, 1762 (1974).
[27]F. Busse, J. Fluid Mech. **52**, 97 (1972).